New recovery based a posteriori error estimators*

C.L. Bottasso[1], G. Maisano[2], S. Micheletti[2], S. Perotto[2]

[1] D. Guggenheim School of Aerospace Engineering
Georgia Institute of Technology
270 Ferst Dr., 30332-0150 Atlanta GA, USA

[2] MOX, Modellistica e Calcolo Scientifico
Dipartimento di Matematica "F. Brioschi"
Politecnico di Milano
via Bonardi 9
I-20133 Milano, Italy

Abstract

In this paper we formulate some new a posteriori recovery-based error estimators. The first one provides us with an improved approximation for the solution gradient. The other two furnish an estimate for the L^2-norm of the error on the solution itself. In more detail, the first estimator is a variant of the well-known Zienckiewicz-Zhu method and it turns out to be exact in 1D for quadratic solutions on non-uniform grids. The second one is based on a solution enrichment relying upon the Zienckiewicz-Zhu recovered gradient. Finally the third estimator consists of a roughening of the solution followed by a Zienckiewicz-Zhu-like recovery applied to the solution itself. The three new proposed methods are compared in terms of their effectivity indices and solution accuracy on two and three dimensional problems.

Keywords recovery techniques; a posteriori analysis; error estimators; finite elements

1 Introduction

Among the various a posteriori error estimation techniques developed in recent years, one of the most widely used in practice is that proposed by Zienckiewicz and Zhu in a series of papers appeared in the late 80's and early 90's [19, 20, 21, 22]. The basic idea behind the Zienckiewicz-Zhu (ZZ) estimators is remarkably simple, and is based on the observation that in a displacement-based finite element method the gradient σ_h is obtained by differentiation of the solution u_h. Hence, the derived fields (e.g., stresses) are less accurate than the primary ones (e.g., displacements). Motivated by this fact, one then reconstructs an improved gradient σ_h^* by re-interpolating in a suitable way the

*This work has been supported by the COFIN 2003 Project "Numerical Models for Advanced Applications in Fluid Dynamics and Electromagnetism".

quantity σ_h. In other words, the original gradient is projected onto a richer space, a recovery process that can be conducted in several different ways [15, 21]. The L^2-norm of the difference between the reconstructed "improved" gradient and the original "rough" one, yields an estimate of the solution error in the energy norm.

The popularity of this methodology can be attributed to various factors: the method is rather independent of the problem, of the governing equations and of most details of the finite element formulation (except for the finite element space), it is cheap to compute and easy to implement and, first and foremost, the method works very well in practice (see, e.g., [2, 8, 12]). On the other hand, we remark that the theoretical properties of this recovery procedure are not very well understood yet, though many theoretical investigations have been carried out in the literature [4, 6, 7, 11, 13, 17, 18].

In this paper we explore the possibility of using some alternative forms of recovery for formulating a posteriori error estimators. All the methods discussed here share with the ZZ approach the generality, low computational cost and ease of implementation. In particular, we consider three different formulations of the error estimator. The first one, discussed in Section 2, is a member of the general family of ZZ estimators: the gradient re-interpolation is based here on a choice of weighting coefficients that ensures the exact reconstruction of the gradient associated with a quadratic solution on non-uniform meshes in one dimension.

Next, in Sections 3 and 4 we discuss new procedures that directly operate on the solution itself, rather than on the gradient as in the ZZ case. In more detail, in Section 3 we propose an error estimator employing an enriched solution. The idea is first to reconstruct the improved gradient σ_h^* using a ZZ procedure, and then to compute an enriched solution u_h^* using u_h and the integral of σ_h^*. For example, if u_h is piecewise linear, since the reconstructed σ_h^* is also linear, we obtain a piecewise quadratic improved u_h^*. The L^2-norm of the difference between the recovered and the original solution yields an estimate of the solution error in the L^2-norm.

In Section 4 the idea is first to compute a "roughened" solution $\bar{u}_h$ from u_h, by projecting u_h onto a poorer space. Next, the rough solution is improved using a ZZ reconstruction, yielding a new solution $\tilde{u}_h$. For example, starting from a piecewise linear u_h we first roughen it by averaging at the element level obtaining a piecewise constant $\bar{u}_h$, and then we ZZ-reconstruct it obtaining a linear $\tilde{u}_h$. The L^2-norm of the difference between the reconstructed $\tilde{u}_h$ and the original u_h, combined with the ZZ estimator, yields an estimate of the solution error in the L^2-norm.

In Section 5 the three new proposed estimators are applied to some representative examples in two dimensions. In particular the estimators are characterized in terms of their effectivity indices and are validated on a mesh adaption procedure.

In Section 6 we focus on hyperbolic problems, such as the Euler equations, exhibiting solutions with shocks. For this kind of problems we devise suitable conditions which allow us to localize the shock inside a given element of the mesh and we modify accordingly the definition of the three error estimators.

Section 7 is finally devoted to the assessment of the error estimators on challenging aerospace problems.

2 A Zienkiewicz-Zhu like recovery procedure

Let us assume as reference problem the following general one: find u such that

$$\begin{cases} Lu = f & \text{in } \Omega, \\ Bu = g & \text{on } \partial\Omega, \end{cases} \tag{1}$$

where L and B are suitable differential operators, possibly nonlinear, f and g are the data of the problem and the computational domain Ω is an open bounded subset of $\mathbb{R}^d$, with $d = 1, 2, 3$, $\partial\Omega$ being its boundary. Problem (1) may be considered as the standard Poisson problem or the linear elasticity problem, though other problems fit this framework.
Let $\mathcal{T}_h = \{K_j\}$ be a conformal partition of the domain Ω [5]. Let V_h denote the finite element space consisting of continuous piecewise linear functions, and let $u_h \in V_h$ be the Galerkin approximation to the solution u in (1). Let σ_h denote the piecewise constant gradient or stress of u_h, σ being the corresponding exact value.

The development of the first "smoothing" procedure for the gradient is introduced by Zienkiewicz and Zhu in [19, 20, 21, 22]. With reference to Figure 1, one of the most used forms of the ZZ error estimator is obtained by means of an averaging step followed by an interpolation process. In more detail, the first step computes the nodal value of reconstructed gradient σ_h^* by the formula

$$\sigma_h^*(\boldsymbol{\xi}_i) = \frac{1}{W} \sum_{j=1}^{n} \sigma_h(\mathbf{s}_j) w_j, \tag{2}$$

where j runs over the n sampling points $\mathbf{s}_j$ ($\square$ points), i is the index of the recovery point $\boldsymbol{\xi}_i$ ($\bullet$ point), w_j are suitable weights and $W = \sum_{j=1}^{n} w_j$.

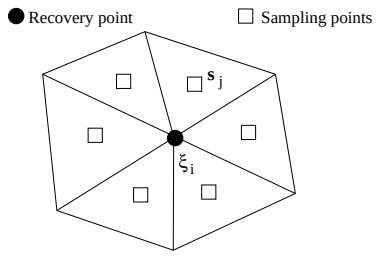

Figure 1: An example of sampling and recovery points in a patch

Then the recovered gradient σ_h^* will be uniquely defined on the space $[V_h]^2$ by a piecewise linear interpolation of the values $\sigma_h^*(\mathbf{x}_i)$. Notice that henceforth we indicate by $\mathbf{x}_i$ the general point of $\mathcal{T}_h$, while we let $\boldsymbol{\xi}_i$ be the same point when used as a recovery point.

Remark 2.1 *As an alternative to the averaging step, a continuous or a discrete least-squares procedure can be used. In this last case the same sampling points as in the averaging phase are usually employed.*

As for the weights w_j, several recipes are available in the literature (e.g. [15]). For instance, we mention just the most employed in practical applications, i.e.

$$w_j = |K_j| \quad \text{or} \quad w_j = \frac{1}{n},$$

$|K_j|$ denoting the area of the triangle containing the sampling point $\mathbf{s}_j$.
In this paper, motivated by the proposition below, we propose the choice

$$w_j = \frac{1}{\|\boldsymbol{\xi}_i - \mathbf{s}_j\|}, \tag{3}$$

where $\|\cdot\|$ stands for the Euclidean norm.

Proposition 2.1 *Let $[a, b]$ be an interval of the real axis decomposed in a non-uniform partition. Then the recovery procedure identified by* (2)-(3) *assures the recovery of the exact gradient of a quadratic u when applied to the piecewise linear interpolant of u.*

Proof. Let $\mathcal{T}_h = \{K_j\}$ be a partition of the interval $[a, b]$, where $K_j = [x_j, x_{j+1})$, with $h_j = x_{j+1} - x_j$ and $x_{j\pm1/2} = (x_{j\pm1} + x_j)/2$ the mid-point of the element K_j (with sign $+$) or K_{j-1} (with sign $-$). Let $\widehat{\sigma}_h$ be the piecewise constant gradient of the linear interpolant function $\Pi_h^1 u$ of u. Notice that, to prove the result, it suffices to check that σ and σ_h^*, recovered starting from $\widehat{\sigma}_h$, coincide at all the nodes x_j, as they are a linear and a piecewise linear function, respectively. We observe that the value of $\widehat{\sigma}_h$ over an element is equal to the exact gradient σ evaluated at the mid-point of the same element, i.e.

$$\widehat{\sigma}_h(x_{j\pm1/2}) = \sigma(x_{j\pm1/2}) \tag{4}$$

(see Figure 2). Applying the recovery procedure (2)-(3), we get

$$\sigma_h^*(\xi_j) = \frac{1}{W}\Big(\widehat{\sigma}_h(x_{j-1/2})w_1 + \widehat{\sigma}_h(x_{j+1/2})w_2\Big). \tag{5}$$

Since, in this case,

$$w_1 = \frac{2}{h_{j-1}}, \qquad w_2 = \frac{2}{h_j}, \qquad W = w_1 + w_2 = \frac{2(h_j + h_{j-1})}{h_j h_{j-1}}, \tag{6}$$

(5) becomes

$$\begin{aligned} \sigma_h^*(\xi_j) &= \frac{h_j h_{j-1}}{2(h_j + h_{j-1})}\Big(\widehat{\sigma}_h(x_{j-1/2})\frac{2}{h_{j-1}} + \widehat{\sigma}_h(x_{j+1/2})\frac{2}{h_j}\Big) \\ &= \frac{h_j\widehat{\sigma}_h(x_{j-1/2}) + h_{j-1}\widehat{\sigma}_h(x_{j+1/2})}{h_j + h_{j-1}}. \end{aligned} \tag{7}$$

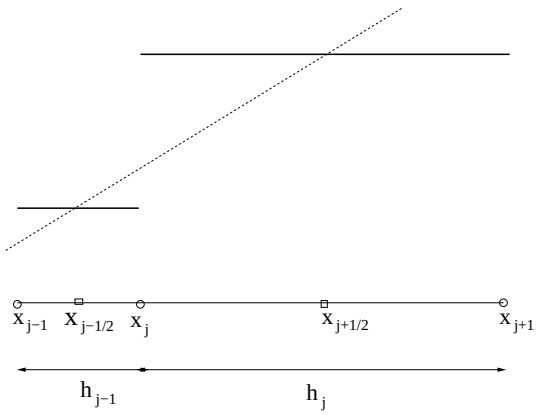

Figure 2: ZZ recovery procedure applied to the piecewise linear interpolant of a quadratic function: σ_h^* (dashed line), $\widehat{\sigma}_h$ (solid line)

On the other hand, the exact gradient σ can be evaluated at the point x_j moving from the equation of the straight line joining the points $(x_{j-1/2}, \sigma(x_{j-1/2}))$ and $(x_{j+1/2}, \sigma(x_{j+1/2}))$ as

$$\sigma(x_j) = \sigma(x_{j-1/2}) + \frac{\big(\sigma(x_{j+1/2}) - \sigma(x_{j-1/2})\big)}{\Big(\frac{h_j}{2} + \frac{h_{j-1}}{2}\Big)} \frac{h_{j-1}}{2} \tag{8}$$

$$= \frac{h_j \sigma(x_{j-1/2}) + h_{j-1}\sigma(x_{j+1/2})}{h_j + h_{j-1}}. \tag{9}$$

On comparing (7) and (8), and using (4), the thesis follows. □

We note that the weights defined in (3) are also used in [10] to improve the discrete least-squares procedure mentioned in Remark 2.1.

The recovery procedure defined in (2)-(3) prompts us to introduce the first error estimator η_1 considered in this paper:

$$\eta_1 = \|\sigma_h^* - \sigma_h\|_{L_2(\Omega)} \simeq |||u - u_h|||, \tag{10}$$

where $|||\cdot|||$ denotes the suitable energy norm.
To simplify the notations, in the following we introduce the

Definition 2.1 *Let* $\mathbf{a} = \{a_j\}$ *be the vector of the sampled values of a given quantity, and let* $\boldsymbol{w} = \{w_j\}$ *be the vector of the weights. Then the recovery operator defined in* (2) *can be identified with the linear operator* $R_w(\cdot)$ *such that*

$$R_w(\boldsymbol{a}) = \frac{1}{W}\, \boldsymbol{w}^T \boldsymbol{a}, \tag{11}$$

with $W = \sum_{j=1}^{n} w_j$.

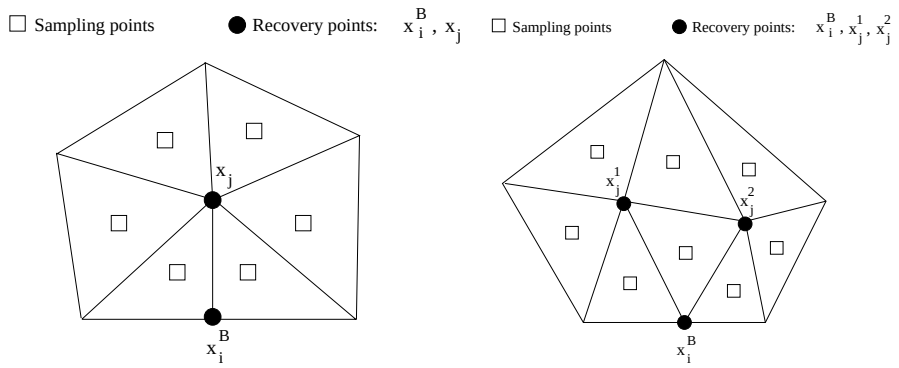

Figure 3: ZZ recovery procedure for the boundary node $\mathbf{x}_i^B$: case of one internal adjacent node (on the left), and of many adjacent internal nodes (on the right)

2.1 Boundary nodes

The recovery procedure of the gradient based either on averaging or on least-squares is not optimal for the nodes on the boundary since an extrapolation process is required. We anticipate the following definitions:

Definition 2.2 *Two nodes are* adjacent *if they share an edge of the mesh.*

Definition 2.3 *For a given mesh node* $\mathbf{y}$*, let* $\mathcal{S}_{\mathbf{y}}$ *denote the set of the standard sampling points associated with* $\mathbf{y}$*.*

As a possible solution to reconstruct the gradient at the boundary nodes, Zienkiewicz and Zhu in [21] suggest using the following procedure (see Figure 3, on the left): for a given boundary node $\mathbf{x}_i^B \in \partial\Omega$,

1. identify the internal node $\mathbf{x}_j$ adjacent to $\mathbf{x}_i^B$;
2. moving from the patch associated with $\mathbf{x}_j$, apply the reconstruction technique to compute the recovered gradient at $\mathbf{x}_i^B$.

In the case when there is more than one internal point adjacent to the boundary node $\mathbf{x}_i^B$ (see Figure 3, on the right), we modify the above procedure in the following way:

1. identify all the internal nodes, say $\mathbf{x}_j^1, \mathbf{x}_j^2$, adjacent to $\mathbf{x}_i^B$;
2. moving from the patch associated with each $\mathbf{x}_j^k$, apply the reconstruction technique to compute the recovered gradient at $\mathbf{x}_i^B$;
3. suitably average the values computed at $\mathbf{x}_i^B$.

As alternative approaches, after computing the recovered gradient at all the internal nodes of the mesh, we propose two different procedures.
Concerning the first one (see Figure 4), we follow the steps below: for a given boundary node $\mathbf{x}_i^B \in \partial\Omega$,

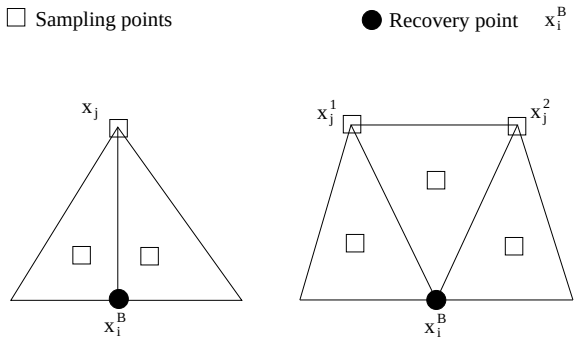

Figure 4: First alternative recovery procedure for the boundary node $\mathbf{x}_i^B$: case of one internal adjacent node (on the left), and of many adjacent internal nodes (on the right)

1. identify all the internal nodes $\mathbf{x}_j$ adjacent to $\mathbf{x}_i^B$;
2. for any $\mathbf{x}_j$, define the new set of sampling points $\mathcal{S}_{\mathbf{x}_j} \cap \mathcal{S}_{\mathbf{x}_i^B} \cup \{\mathbf{x}_j\}$;
3. moving from these new sets of sampling points, apply the reconstruction technique to compute the recovered gradient at $\mathbf{x}_i^B$;
4. suitably average the values computed at $\mathbf{x}_i^B$.

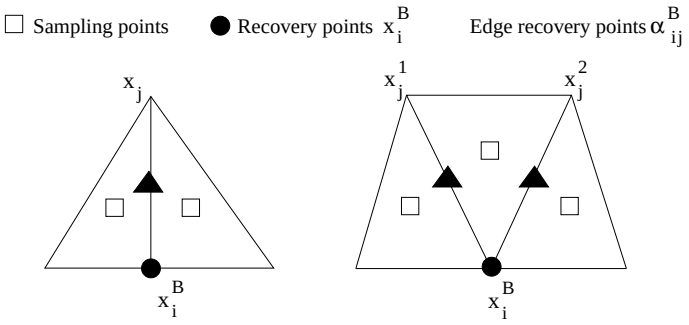

Figure 5: Second alternative recovery procedure for the boundary node $\mathbf{x}_i^B$: case of one internal adjacent node (on the left), and of many adjacent internal nodes (on the right)

The second approach consists of the following items (see Figure 5): for a given boundary node $\mathbf{x}_i^B \in \partial\Omega$,

1. identify all the internal nodes $\mathbf{x}_j$ adjacent to $\mathbf{x}_i^B$;

2. average the values at the sampling points of the two triangles sharing edge $\overline{\mathbf{x}_i^B\mathbf{x}_j}$ and assign this value to the mid-point α_{ij}^B of the edge $\overline{\mathbf{x}_i^B\mathbf{x}_j}$;

3. extrapolate linearly the two values of the recovered gradient at $\mathbf{x}_j$ and α_{ij}^B to $\mathbf{x}_i^B$;

4. suitably average the values computed at $\mathbf{x}_i^B$.

3 The enriching-recovery technique for the solution

In this section we introduce the first new error estimator η_2 for the norm $\|e_h\|_{L^2(\Omega)}$. All the information provided by the improved gradient σ_h^* defined in the previous section are used to obtain an enriched piecewise quadratic approximation u_h^* to u_h, starting point for the construction of η_2.
Due to the quadratic nature of the recovered quantity u_h^*, it suffices to compute it at the vertices and at the mid-points of the edges of $\mathcal{T}_h$, following the recovery procedure below (see Figure 6, on the left):

1. set the values of u_h^* at the vertices as $u_h^*(\mathbf{x}_i) = u_h(\mathbf{x}_i)$;

2. let $\boldsymbol{\xi}_{ij}$ be the mid-point of the edge with vertices $\mathbf{x}_i$ and $\mathbf{x}_j$. Compute the two values
$$\begin{aligned} \Xi_{ij}^1 &= u_h(\mathbf{x}_i) + \frac{(\boldsymbol{\xi}_{ij} - \mathbf{x}_i)^T}{\|\boldsymbol{\xi}_{ij} - \mathbf{x}_i\|} \int_{\mathbf{x}_i}^{\boldsymbol{\xi}_{ij}} \sigma_h^*\, d\gamma, \\ \Xi_{ij}^2 &= u_h(\mathbf{x}_j) + \frac{(\boldsymbol{\xi}_{ij} - \mathbf{x}_j)^T}{\|\boldsymbol{\xi}_{ij} - \mathbf{x}_j\|} \int_{\mathbf{x}_j}^{\boldsymbol{\xi}_{ij}} \sigma_h^*\, d\gamma. \end{aligned} \tag{12}$$
   Notice that the line integrals in (12) are carried along the edge and are exactly computable by the mid-point quadrature rule.

3. assign to u_h^* at the mid-point $\boldsymbol{\xi}_{ij}$ the value $u_h^*(\boldsymbol{\xi}_{ij})$ given by the arithmetic average of Ξ_{ij}^1 and Ξ_{ij}^2;

4. interpolate the values of u_h^* at the vertices and at the mid-points by the standard piecewise quadratic shape functions.

Remark 3.1 *Notice that when the approximations u_h and σ_h^* in* (12) *coincide with the exact quantities u and σ, respectively, it holds also that $\Xi_{ij}^1 = \Xi_{ij}^2 \equiv u(\boldsymbol{\xi}_{ij})$.*

Remark 3.2 *We point out that if a scalar function ϕ exists such that $\sigma_h^* = \nabla\phi$, then the recovery procedure just above would provide us with $u_h^* = \phi$. In general, the ZZ recovery procedure does not guarantee that this is the case, so that Ξ_{ij}^1 and Ξ_{ij}^2 differ as they depend on the integration path.*

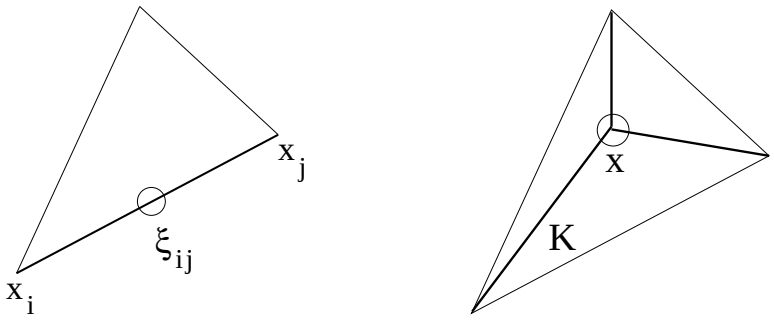

Figure 6: Enriching-recovery procedure: recovery at the mid-edge $\boldsymbol{\xi}_{ij}$ (on the left) and at the internal point $\mathbf{x}$ (on the right)

A theoretical analysis of the accuracy properties of this recovery procedure is provided in the Appendix for the 1D case.

The error indicator η_2 associated with this recovery procedure is given by:

$$\eta_2 = \|u_h^* - u_h\|_{L_2(\Omega)} \simeq \|u - u_h\|_{L_2(\Omega)}. \tag{13}$$

Remark 3.3 *The piecewise reconstruction above can be extended for computing the value of u_h^* at any point $\mathbf{x} \in K$, for any K in $\mathcal{T}_h$, by averaging the value of the three line integrals along the segments joining $\mathbf{x}$ with the vertices of K (see Figure 6, on the right). However in such a case u_h^* is no longer a piecewise quadratic function.*

4 The roughening-recovery technique for the solution

The recovery technique introduced in Section 2 is one of the main ingredients used to define the second new error estimator η_3 for the L^2-norm of the discretization error. The other principal tool is a suitable piecewise linear reconstruction $\widetilde{u}_h$ of the discrete solution u_h.
Let us detail the procedure adopted to build the recovery quantity $\widetilde{u}_h$:

1. a piecewise constant solution $\bar{u}_h$ is obtained via a *roughening* procedure, such that $\bar{u}_h|_{K_j} = \bar{u}_j$, with
$$\bar{u}_j = \frac{\displaystyle\int_{K_j} u_h \, d\mathbf{x}}{|K_j|}; \tag{14}$$

2. the recovery operator R_w identified in Definition 2.1, for the choice $a_j = \bar{u}_j$, is used in order to produce the nodal values $\tilde{u}_h(\boldsymbol{\xi}_i)$ (see Figure 1):
$$\tilde{u}_h(\boldsymbol{\xi}_i) = R_w(\boldsymbol{a}); \tag{15}$$

3. the reconstruction $\tilde{u}_h$ is finally uniquely defined on the space V_h by piecewise linearly interpolating the values $\tilde{u}_h(\boldsymbol{\xi}_i)$.

The local error estimator associated with this procedure is defined as:

$$\eta_{3,K} = \frac{\mu}{2}\left(\|\widetilde{u}_h - u_h\|_{L^2(K)} + h_K\|\sigma_h^* - \sigma_h\|_{L^2(K)}\right) \simeq \|u - u_h\|_{L^2(K)}, \tag{16}$$

h_K being the diameter of element K. In more detail the local estimator is an average of two dimensionally homogeneous terms thanks to the weight h_K.

Remark 4.1 *The choice of averaging the two norms in* (16) *aims at balancing their estimating properties, since the numerical results show that the first one* ($\|\widetilde{u}_h - u_h\|_{L^2(K)}$) *over-estimates the true error around maxima and minima of the solution, while the second one* ($\|\sigma_h^* - \sigma_h\|_{L^2(K)}$) *does the other way around.*

The scaling factor μ has been chosen equal to $4/7$ by tuning it on a simple reference problem. Let u be a quadratic function, $u_h = \Pi_h^1(u)$ the linear interpolant of u and $\mathcal{T}_h$ a regular structured mesh (that is, $h_K = H$ for any K). Then

$$\mu \simeq \frac{2\,\|u - u_h\|_{L_2(K)}}{\|\widetilde{u}_h - u_h\|_{L_2(K)} + h_K\|\sigma_h^* - \sigma_h\|_{L_2(K)}} = \frac{4}{7}, \tag{17}$$

with $\widetilde{u}_h$, σ_h^* and σ_h defined as in the previous sections.
Finally the global error estimator η_3 is obtained by summing up the local contributions as

$$\eta_3 = \Big(\sum_{K\in\mathcal{T}_h} \eta_{3,K}^2\Big)^{1/2}.$$

5 Numerical studies in 2D

In this section we report on numerical studies in 2D about some problems whose exact solution is avaiable. In particular, we study the robustness of the above error indicators both on a sequence of regularly refined meshes and on iteratively adapted grids.

5.1 Study of the effectivity index

In order to evaluate the robustness of the error indicators η_i, one of the main quantities usually monitored is the so-called *effectivity index* θ_i, defined by

$$\theta_i = \frac{\eta_i}{\|u - u_h\|_i}, \tag{18}$$

where $\|\cdot\|_i \equiv |||\cdot|||$ for $i = 1$ and coincides with the L^2-norm for $i = 2, 3$ [21]. We recall that an error indicator is *asymptotically exact* if the corresponding effectivity index converges to one as $h \to 0$, where $h = \max_{K\in\mathcal{T}_h} h_K$.

Let us consider in the following the reference problem (1) with $L = -\Delta$ and $B = I$, the Laplacian and the indentity operators, respectively.
Only regular meshes are used and three different test-cases are considered whose exact solutions are given by

$$u_1 = 1 + (x^2 + y^2)\sin(20xy) \qquad \text{in } \Omega = (0,1) \times (0,1), \tag{19}$$

$$u_2 = 1 + (x^2 + y^2)\sin(xy) \qquad \text{in } \Omega = (3,5) \times (0,1), \tag{20}$$

$$u_3 = xy(1-x)(1-y) \qquad \text{in } \Omega = (0,1) \times (0,1), \tag{21}$$

respectively, the right-hand side f and the boundary datum g being chosen accordingly. First we apply the error indicators on regular structured meshes. The behaviour of the effectivity indeces θ_i as a function of $\log_{10}(1/h)$ are tabulated in Tables 1 - 3, for the three test-cases. Note that all the three effectivity indeces show a saturation trend as $h \to 0$, though only $\theta_1 \to 1$.

Table 1: Effectivity indeces associated with the first test-case on a structured regular mesh

$log_{10}(1/h)$	θ_1	θ_2	θ_3
1.150	0.8418	0.4106	0.5263
1.451	1.0112	0.5654	0.6885
1.752	1.0197	0.6770	0.7635
2.053	1.0074	0.7193	0.7943
2.354	1.0021	0.7313	0.8059

Table 2: Effectivity indeces associated with the second test-case on a structured regular mesh

$log_{10}(1/h)$	θ_1	θ_2	θ_3
1.000	1.0241	0.7831	1.0821
1.315	1.0102	0.8195	1.1295
1.652	1.0053	0.8251	1.1622
1.913	1.0005	0.8271	1.1727
2.232	1.0001	0.8289	1.1809

Table 3: Effectivity indeces associated with the third test-case on a structured regular mesh

$log_{10}(1/h)$	θ_1	θ_2	θ_3
1.150	0.9954	0.7691	0.8791
1.451	1.0001	0.7748	0.9105
1.752	1.0000	0.7751	0.9251
2.053	1.0000	0.7755	0.9340
2.354	1.0000	0.7756	0.9406

The same test-cases have been solved on regularly refined unstructured meshes. In Tables 4 - 6 we show only the values of θ_1 and θ_2, since η_3 tends to over-estimates the error. However, when applied to adaptively refined meshes this estimator generates reasonable grids too, both in the 2D and in 3D case (see Sections 5.2 and 7).

Table 4: Effectivity indeces associated with the first test-case on a regularly refined unstructured mesh

$log_{10}(1/h)$	θ_1	θ_2
0.699	1.0526	0.6089
1.000	1.0567	0.8419
1.301	1.0216	0.9095
1.602	1.0051	0.9249
1.903	1.0001	0.9230

Table 5: Effectivity indeces associated with the second test-case on a regularly refined unstructured mesh

$log_{10}(1/h)$	θ_1	θ_2
0.523	1.0293	1.0418
0.824	1.0060	1.0470
1.125	1.0011	1.0223
1.426	0.9987	1.0334
1.727	0.9975	1.0323

Table 6: Effectivity indeces associated with the third test-case on a regularly refined unstructured mesh

$log_{10}(1/h)$	θ_1	θ_2
0.699	1.0094	0.9724
1.000	1.0008	0.9669
1.301	1.0004	0.9784
1.602	0.9985	0.9706
1.903	0.9985	0.9840

5.2 The adaptive refinement procedure

In this section we use the three error indicators η_i for an adaptive refinement procedure. Let us introduce the *local percentage error indicator* defined by

$$\eta_i^{\%} = \frac{\eta_i}{\frac{\|u_h\|_{i(K)} + u_m}{2}}, \quad \text{with} \quad i = 1, 2, 3, \tag{22}$$

where

$$u_m = \Big(\frac{\|u_h\|_i^2}{N}\Big)^{1/2}, \tag{23}$$

N being the number of triangles of the current mesh. For a given test-case, let ϵ_i be the tolerance associated with the error indicator η_i. Then our adaptive procedure consists of refining the elements satisfying

$$\eta_i^{\%} > \epsilon_i. \tag{24}$$

The model problem is still represented by the Poisson problem (1), the exact solution being now equal to

$$u_4 = x(1-x)y(1-y)\tan^{-1}\Big(\alpha_0\Big(\frac{x+y}{\sqrt{2}} - c_0\Big)\Big) \qquad \text{in } \Omega = (0,1)\times(0,1), \tag{25}$$

where $\alpha_0 = 20$, $c_0 = 0.8$. The right-hand side f and the boundary datum g are chosen accordingly. The initial mesh is the same for all the indicators and consists of 78 elements. In Figure 7 the adapted meshes obtained after $3, 4$ and 4 adaption iterations are shown. The tolerance ϵ_i has been chosen so that the final meshes have about the same number of elements. We note that the mesh obtained with the error estimator η_1 is characterized by a thicker layer around the critical central diagonal zone, compared with the two other grids. In Table 7 the main quantities characterizing the three error estimators are gathered. In particular analyzing the values in the last two rows corresponding to the exact percentage global errors with respect to the L^2-norm and the energy norm, respectively, we observe that while for η_2 and η_3 the tolerances are met, this is not the case for η_1. We may infer that even though the error estimators η_2 and η_3 are a little bit more expensive than η_1, as they both use the recovery procedure yielding η_1, the

adaptive procedures associated with them turn out to be more effective as far as the satisfaction of the global tolerance is concerned.

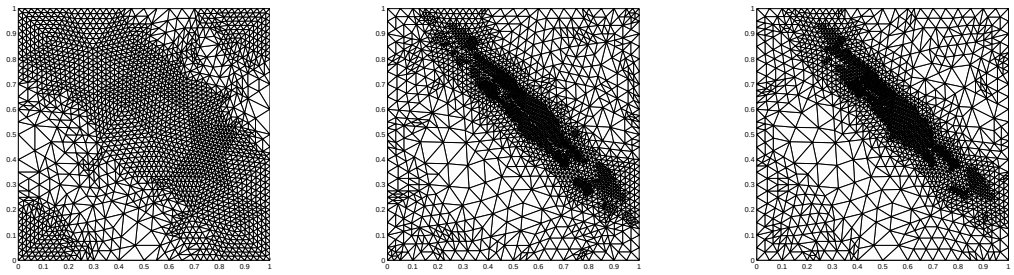

Figure 7: Final adaptive meshes for the fourth test-case: η_1 (left), η_2 (middle), η_3 (right)

Table 7: Main quantities for the fourth test-case

	η_1	η_2	η_3
$\epsilon_i\%$	10	1.6	1.4
θ_1	1.0314	1.0139	1.0155
θ_2	1.0422	1.1319	1.1317
θ_3	0.9261	1.0248	0.9788
n_elem	4111	3999	4206
$\|e_h\|_{L^2(\Omega)}$	$5.81e-04$	$5.46e-04$	$5.26e-04$
$\|\|\|e_h\|\|\|$	$8.96e-02$	$9.28e-02$	$9.16e-02$
$\|e_h\|_{L^2(\Omega)}/\|u_h\|_{L^2(\Omega)}\%$	0.87	0.82	0.79
$\|\|\|e_h\|\|\|/\|\|\|u_h\|\|\|\%$	28.7	29.7	29.3

6 Shock capturing procedures

The recovery procedures leading to the three error estimators η_1, η_2 and η_3 can be extended to the 3D case as well as specialized at capturing shocks. This last feature turns out to be particularly interesting in 3D applications. In more detail we consider in the sequel the Euler equations and we estabilish suitable conditions for detecting the region containing the shock, tipically distributed over a layer with a thickness of 3-4 elements. For the sake of simplicity we explain the shock capturing procedure in a 1D framework, by refering to Figure 8 for a typical situation. Let us assume that the shock occurs somewhere between $x = A$ and $x = B$ (see Figure 8-(a) which shows the numerical solution u_h). The corresponding piecewise constant gradient (solid line) and recovered gradient (dashed line) are plotted in Figure 8-(b). We note that both the two gradients reach their maximum value inside the element $[A, B]$. Moving from this observation we can state the following *Shock Capturing Conditions (SCC)*: for any element $[x_i, x_{i+1}]$,

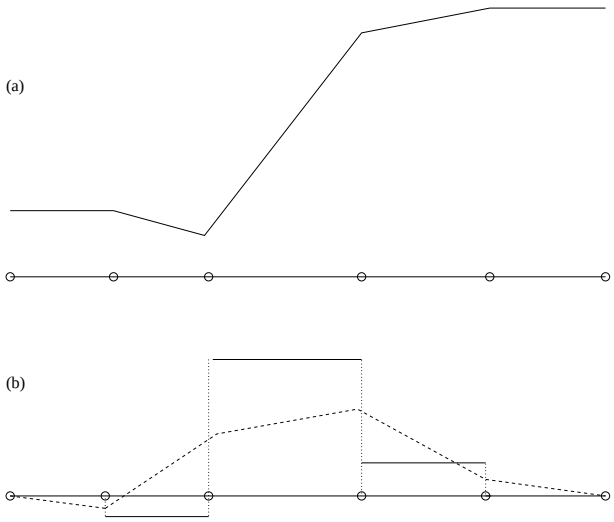

Figure 8: Shock in 1D. (a) the solution; (b) solid line is the gradient, dashed line is the recovered gradient

with $i = 0, ..., n-1$,

$$\begin{cases} |\sigma_h^*(\mathbf{x}_j)| < |\sigma_{h,i}|, \quad j = i, i+1, \\ \dfrac{|\,|\bar{\sigma}_{h,i}^*| - |\sigma_{h,i}|\,|}{|\sigma_{h,i}|} \geq 0.25, \end{cases} \tag{26}$$

where $\sigma_{h,i} = \sigma_h\big|_{[x_i, x_{i+1}]}$ and

$$\bar{\sigma}_{h,i}^* = \frac{\displaystyle\int_{x_i}^{x_{i+1}} \sigma_h^*(x)\, dx}{x_{i+1} - x_i}. \tag{27}$$

The first requirement in (26) demands that all the element nodal values of the recovered gradient be less than the element constant value $\sigma_{h,i}$, where the absolute value is understood. Moreover the second condition requires that the jump between the averaged recovered gradient and the constant value $\sigma_{h,i}$ be at least the 25% of $\sigma_{h,i}$.

Remark 6.1 *Notice that the SCC can be readily carried over to the d-dimensional case, with $d = 2, 3$, simply by substituting in* (26) *the absolute values with the Euclidean norm and by letting j running over all the nodes of the generic element.*

We point out that, even though SCC may be satisfied over an element not containing a real shock, this is no longer the case when further refining the mesh.

6.1 The shock capturing error indicators

In order to deal with the presence of a shock we have to suitably modify the error indicators η_1, η_2 and η_3 previously defined in all the elements satisfying the SCC. Namely,

we impose

$$\sigma_h^*(\mathbf{x}_j) = 0 \quad j = i, i+1. \tag{28}$$

Concerning the error indicator η_1, its definition does not change after the constraints (28). As for η_2, the local error estimator $\eta_{2,K}$ becomes

$$\eta_{2,K} = \mu \frac{\gamma \|\widetilde{u}_h - u_h\|_{L^2(K)} + h_K \|\sigma_h^* - \sigma_h\|_{L_2(K)}}{2}, \tag{29}$$

where $\gamma = 2$ for the 1D case while $\gamma = d + 1$ for the d-dimensional case. Moreover $K = [x_i, x_{i+1}]$ and $h_K = x_{i+1} - x_i$ for the one-dimensional case.
As for the third error estimator η_3, some further modifications are required. This is due to the fact that if we recover the value of u_h^* only at the mid-point on each interval K, we obtain that $u_h^* \equiv u_h\big|_K$, because of (28). Since this condition implies the wrong conclusion $\eta_{3,K} = 0$, we suggest the following modification: reconstruct u_h^* not only at the mid-point $\boldsymbol{\xi}_{i2}$ but also at two other points $\boldsymbol{\xi}_{i1}$ and $\boldsymbol{\xi}_{i3}$ (at least) symmetrically distributed over the element K, using the procedure defined in (12). This yields a total of two values $u_h^*(\boldsymbol{\xi}_{ik}^-)$ (left) and $u_h^*(\boldsymbol{\xi}_{ik}^+)$ (right), for each of the three points $\boldsymbol{\xi}_{ik}$. The final value of u_h^* at point $\boldsymbol{\xi}_{ik}$ is obtained by averaging the left and right values as

$$u_h^*(\boldsymbol{\xi}_{ik}) = \frac{1}{W} \left(w_k^- \, u_h^*(\boldsymbol{\xi}_{ik}^-) + w_k^+ \, u_h^*(\boldsymbol{\xi}_{ik}^+) \right)$$

where

$$w_k^- = \frac{1}{\|\mathbf{x}_i - \boldsymbol{\xi}_{ik}\|^s}, \quad w_k^+ = \frac{1}{\|\mathbf{x}_{i+1} - \boldsymbol{\xi}_{ik}\|^s} \tag{30}$$

and $W = w_k^- + w_k^+$ with $k = 1, 2, 3$. Notice that the choice $s >> 1$, e.g. $s = 20$, introduces the correct "upwinding" effect. (see Figure 9).

7 A numerical validation in 3D

The application of the three estimators to 3D test-cases is still under investigation. In particular we just provide two preliminary results obtained using only the estimator η_2 modified according to the *SCC*.
The reference problem (1) is now identified with the compressible Euler equations completed with suitable boundary conditions. In the first test-case we consider a supersonic flow around an ogive with incidence angle $\alpha = 10°$, asymptotic Mach and Reynolds numbers $M_\infty = 2.00$, $Re_\infty = 5.33e06$, respectively and asymptotic temperature and pressure $T_\infty = 183.3K$, $p_\infty = 6390Pa$.

In Figure 10 the final mesh is shown after three adaption steps. The shock wave under the ogive as well as the rarefaction wave above the ogive are well captured . The over-refinement about the surface of the ogive can be justified by the presence of a vortex starting from the cone. Due to the three-dimensional nature of this test-case and to the complexity of the simulated phenomenon, a great number of elements may be easily generated. The mesh in Figure 10 has more than 2,7 millions of elements. Thus it is mandatory to have an error estimator minimizing the number of elements generated

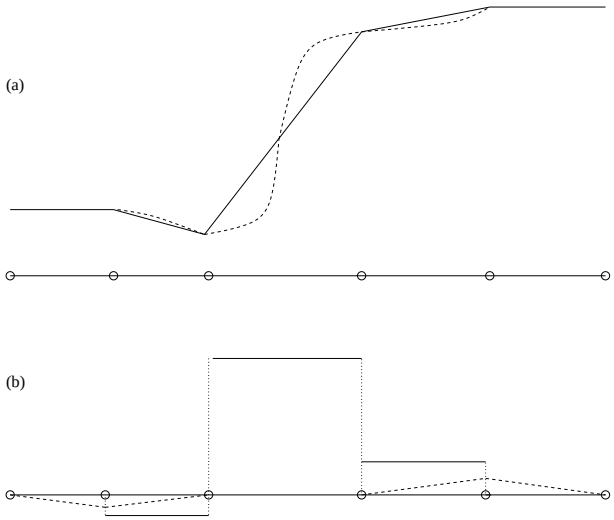

Figure 9: Shock in 1D. (a) solid line is the solution calculated, dashed line is the recovered solution obtained by η_3. (b) solid line is the gradient, dashed line is the recovered gradient

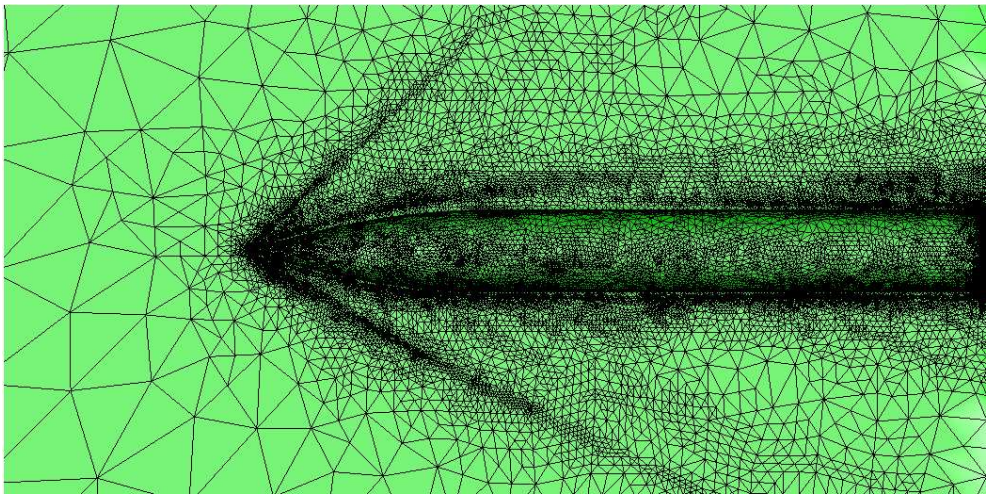

Figure 10: Final adaptive mesh for the ogive test-case

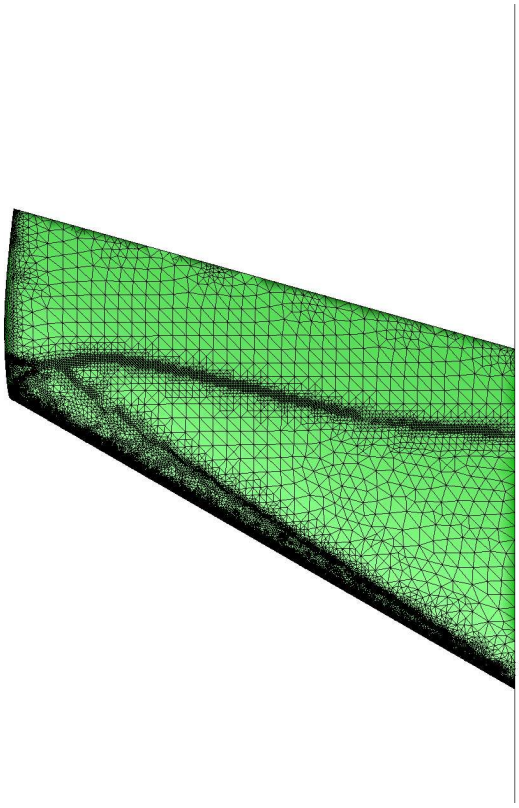

Figure 11: Final adaptive mesh for the Onera test-case

during the adaption process. In the second test-case we consider the classical Onera problem (see [16] for all the details). The asymptotic Mach and Reynolds numbers have been chosen as $M_\infty = 0.8395$, $Re_\infty = 11.72e06$, respectively while the angle of attack and the angle of sideslip are set $\alpha_1 = 3.06^\circ$ and $\alpha_2 = 0.0^\circ$. The mesh in Figure 11 highlights the presence of the λ-shock and consists of about 2.3 million of elements.

In this section we prove a result about the consistency and the accuracy of the recovery procedure provided in Section 3 in the 1D case (see [9]).

Proposition .1 *Let $I_a^b(f)$ be the approximation of the exact integral $\int_a^b f\,dx$ provided by the mid-point quadrature rule. Let $\beta = (\alpha+\gamma)/2$ be the mid-point of the interval (α,γ). If $f \in \mathbb{P}^3([\alpha,\gamma])$, then the approximated value*

$$f^*(\beta) = \frac{1}{2}\big(f(\alpha) + I_\alpha^\beta(f')\big) + \frac{1}{2}\big(f(\gamma) - I_\beta^\gamma(f')\big) \tag{31}$$

coincides with the exact value $f(\beta)$. In general, if f is smooth enough, we have

$$e(\beta) = f(\beta) - f^*(\beta) = \mathcal{O}(H^4), \tag{32}$$

where $H = (\gamma-\alpha)/2$.

Proof. It is known that, for f smooth enough,

$$f(\beta) - f(\alpha) = \int_\alpha^\beta f'(x)\,dx \quad \text{and} \quad f(\beta) - f(\gamma) = -\int_\beta^\gamma f'(x)\,dx. \tag{33}$$

Usually the integrals above can not be computed exactly. Thus a suitable quadrature rule is required. Let us adopt in the sequel the mid-point rule. By summing the two equations in (33), we get

$$\begin{aligned} f(\beta) &= \frac{1}{2}\left(f(\alpha) + \int_\alpha^\beta f'(x)\,dx + f(\gamma) - \int_\beta^\gamma f'(x)\,dx\right) \\ &= \frac{1}{2}\left(f(\alpha) + I_\alpha^\beta(f') + f(\gamma) - I_\beta^\gamma(f') + E_I^{(\alpha,\beta)} - E_I^{(\beta,\gamma)}\right), \end{aligned} \tag{34}$$

where we have taken into account the quadrature errors

$$\begin{aligned} E_I^{(\alpha,\beta)} &= \int_\alpha^\beta f'(x)dx - I_\alpha^\beta(f') = \frac{H^3}{24}f'''(\varsigma_1), \\ E_I^{(\beta.\gamma)} &= \int_\beta^\gamma f'(x)dx - I_\beta^\gamma(f') = \frac{H^3}{24}f'''(\varsigma_2), \end{aligned} \tag{35}$$

where $\varsigma_1 \in (\alpha,\beta)$ and $\varsigma_2 \in (\beta,\gamma)$. Combining (31) with (34), we have:

$$f(\beta) = f^*(\beta) + \frac{1}{2}(E_I^{(\alpha,\beta)} - E_I^{(\beta,\gamma)}). \tag{36}$$

Let us choose $f \in \mathbb{P}^3([\alpha,\gamma])$, thus characterized by a constant third order derivative, i.e. $f'''(\varsigma_1) = f'''(\varsigma_2) \equiv C_1$. Thanks to (35), the equality $f(\beta) = f^*(\beta)$ immediately follows.

Now, let f be any smooth function in $[\alpha,\gamma]$. From (36) and (35) and exploiting the regularity of f, we obtain

$$f(\beta) = f^*(\beta) + \frac{H^3}{48}(f'''(\varsigma_1) - f'''(\varsigma_2)) = f^*(\beta) + \frac{H^3}{48}(\varsigma_1 - \varsigma_2)f^{IV}(\varsigma), \tag{37}$$

with $\varsigma \in (\varsigma_1,\varsigma_2)$, where the Taylor expansion of $f'''(\varsigma_1)$ about ς_2 has been exploited. Noticing that, as $|\varsigma_1 - \varsigma_2| \le 2H$, we have

$$|e(\beta)| = |f(\beta) - f^*(\beta)| \le C_2\,H^4, \tag{38}$$

where C_2 depends on the fourth order derivative of f. □

References

[1] Ainsworth M, Oden JT. *A Posteriori Error Estimation in Finite Element Analysis.* John Wiley & Sons, Inc: New-York, 2000.

[2] Bruch JC. Free surface seepage problems solved using: a) the Zienkiewicz-Zhu error estimation procedure; and b) a parallel computer. *Pitman Res. Notes Math. Ser.* 1993; **282**: 98-104.

[3] Becker R, Rannacher R. An optimal control approach to a posteriori error estimation in finite element methods. *Acta Numerica* 2001; **10**: 1–102.

[4] Carstensen C, Bartels S. Each averaging technique yields reliable a posteriori error control in FEM on unstructured grids. I: Low order conforming, nonconforming, and mixed FEM. *Math. Comp.* 2001; **71**: 945–969.

[5] Ciarlet Ph. *The Finite Element Method for Elliptic Problems*. North-Holland Publishing Company: Amsterdam, 1978.

[6] Krízek M, Neittaanmäki P. Superconvergence phenomenon in the finite element method arising from averaging gradients. *Numer. Math.* 1984; **45**: 105–116.

[7] Krízek M, Neittaanmäki P. On a global superconvergence of the gradient of linear triangular elements. *J. Comput. Appl. Math.* 1987; **18**: 221–233.

[8] Lawrence KL, Nambiar RV. The Zienkiewicz-Zhu error estimator for multiple material problems. *Commun. Appl. Numer. Methods* 1992; **8**(4): 273-277.

[9] Maisano G. A posteriori error estimator methods based on recovery techniques (in italian). *Degree thesis*, Politecnico di Milano 2004.

[10] Mavriplis DJ. Revisiting the least-square procedure for gradient reconstruction on unstructured meshes. *NASA/CR Report* 2003-06, 2003.

[11] Micheletti M, Perotto S. Reliability and efficiency of an anisotropic Zienkiewicz-Zhu error estimator. submitted for the publication in *Comput. Methods Appl. Mech. Engrg.* 2004.

[12] Pawlak TP, Wheeler MJ, Yunus SM. Application of the Zienkiewicz-Zhu error estimator for plate and shell analysis. *Int. J. Numer. Methods Eng.* 1990; **29**(6): 1281-1298.

[13] Picasso M. Numerical study of the effectivity index for an anisotropic error indicator based on Zienkiewicz-Zhu error estimator. *Comm. Numer. Methods. Engrg.* 2003; **19**(1): 13–23.

[14] Quarteroni A, Valli A. *Numerical Solution of Partial Differential Equations*. Springer Verlag: New York, 1997.

[15] Rodríguez R. Some remarks on Zienkiewicz-Zhu estimator. *Numer. Methods Partial Differential Equations* 1994; **10**(5): 625–635.

[16] Schmitt V, Charpin F. Pressure distributions on the ONERA-M6-Wing at transonic Mach numbers. Report of the Fluid Dynamics Panel Working Group 04, AGARD AR 138, 1979.

[17] Yan N, Zhou A. Gradient recovery type a posteriori error estimation for finite element approximations on irregular meshes. *Comput. Methods Appl. Mech. Engrg.* 2001: **190**: 4289–4299.

[18] Zhang Z, Zhu JZ. Superconvergence of the derivative patch recovery technique and *a posteriori* error estimation. In the *IMA Volumes in Mathematics and its Applications*, Babuska I, Flaherty JE, Henshaw WD, Hopcroft JE, Oliger JE, Tezduyar T (eds). Modeling, Mesh Generation, and Adaptive Numerical Methods for Partial Differential Equations, Springer-Verlag: New York, 1995; bf 75: 431–450.

[19] Zienkiewicz OC, Zhu JZ. A simple error estimator and adaptive procedure for practical engineering analysis. *Int. J. Numer. Meth. Engng.* 1987; **24**(2): 337–357.

[20] Zienkiewicz OC, Zhu JZ. The superconvergent patch recovery (SPR) and adaptive finite element refinement. *Comput. Methods Appl. Mech. Engrg.* 1992; **101**(1-3): 207–224.

[21] Zienkiewicz OC, Zhu JZ. The superconvergent patch recovery and a posteriori error estimates. I: The recovery technique. *Int. J. Numer. Meth. Engng.* 1992; **33**(7): 1331–1364.

[22] Zienkiewicz OC, Zhu JZ. The superconvergent patch recovery and a posteriori error estimates. II: Error estimates and adaptivity. *Int. J. Numer. Meth. Engng.* 1992; **33**(7): 1365–1382.